Proceedings of the 20th International Conference on Soil Mechanics and Geotechnical Engineering– Rahman and Jaksa (Eds)

SLIDE-PM: a 2D-FEM prototype to quantify the vulnerability of buildings with respect to mud flows

SLIDE-PM : Un prototype 2D-FEM pour la quantification de la vulnérabilité des bâtiments soumis aux coulées de boue

Colette Jost & Stéphane Commend
iTEC, University of Applied Sciences and Arts Western Switzerland, Fribourg, Switzerland, colette.jost@hefr.ch

Jacopo Abbruzzese, Tanja Miteva & Erika Prina Howald
insit, University of Applied Sciences and Arts Western Switzerland, Yverdon-les-Bains, Switzerland

ABSTRACT: The design of protection measures against mud flows is usually justified by the vulnerability of a given building due to a possible event. Empirical approaches, hard to quantify, are often used. A new tool prototype is therefore developed, which allows quantifying the vulnerability based on three consecutive 2D finite element models. A first model, taking into account the topology, stratigraphy and hydrogeological conditions is used to identify the rupture mechanism and therefore the size and shape of the resulting mudflow. Afterwards, the triggered volume is propagated along the slope using a second model and the impact force is quantified. Finally, this force is applied on a third nonlinear structural model. The vulnerability of the building is then estimated based on the resulting force-displacement curve. The propagation of the triggered volume and the calculation of the impact force is validated on a granular flow laboratory experiment. Then a real-life case study, an event in Wenjia Gully (China) is simulated. The identification of the failure mechanism compared to existing models of this event. Finally, vulnerability to this event of different fictitious buildings is evaluated.

RÉSUMÉ : La conception de mesures de protection contre les coulées de boue est généralement justifiée par la vulnérabilité d'un bâtiment donné soumis à un événement possible. Souvent des approches empiriques, difficiles à quantifier, sont utilisées. Un nouveau prototype d'outil est donc développé, qui permet de quantifier la vulnérabilité sur la base de trois modèles d'éléments finis 2D consécutifs. Un premier modèle, tenant compte de la topologie, de la stratigraphie et des conditions hydrogéologiques, est utilisé pour identifier le mécanisme de rupture et donc la taille et la forme de la coulée de boue résultante. Le volume déclenché est propagé à l'aide d'un deuxième modèle et la force d'impact est quantifiée. Enfin, cette force est appliquée sur un troisième modèle structurel non linéaire. La vulnérabilité du bâtiment est alors estimée sur la base de la courbe force-déplacement résultante. La propagation du volume déclenché et le calcul de la force d'impact sont validés sur une expérience de laboratoire d'écoulement granulaire. Ensuite, on simule un évènement au ravin de Wenjia (Chine). L'identification du mécanisme de rupture est comparée aux modèles existants de cet événement. Enfin, la vulnérabilité de différents bâtiments fictifs à cet événement est évaluée.

KEYWORDS: Numerical Methods; Soil-Structure Interaction and Retaining Walls; Slope Stability in Engineering Practice

1 INTRODUCTION

The determination of possible damages on a structure due to natural hazards is an important task, as risk assessment is necessary in order to design appropriate protection measures. In this context, the quantification of the vulnerability of the structure to be protected against a possible event is necessary.

In this work, we focus on mud flows caused by a slope instability as shown in Figure 1. Heavy rainfall leads to an increase in groundwater level. The succeeding increase in pore pressure causes a slope failure. The mobilized material forms a mud flow propagating downhill. Eventually this mud flow hits and damages a structure placed downhill. Other triggering actions as continuous erosion are not considered in this paper.

In this context historical-empirical and qualitative approaches are often used. For example, (Blahut, Glade and Sterlacchini 2014, Mavrouli, et al. 2014, Ciurean, et al. 2017) present quantification methods based on the type of structure, resistance parameters and intensity parameters. (Cardinali, et al. 2002) explores the risk of future instabilities based on aerial photographs and in-situ measurements. The application of such models requires profound understanding of the processes going on. Especially intensity parameters are hard to estimate, as they model the outcome of a complex process on a simple value.

The goal of this ongoing project is to develop a prototype tool, which allows quantifying the vulnerability based on three consecutive 2D finite element models. The aim of the use of numerical simulations is to allow the modelling of a relatively complex process with possibly non-trivial inputs as the slope's geometry or the structure, keeping the input parameters as physical-based and straightforward as possible.

In this paper, the calculation method and the prototype tool are presented and the method is validated. The propagation of a triggered volume as well as the calculation of the impact force is validated on a flume experiment with dry sand (Moriguchi, et al. 2009). A real life example in Wenjia gully, China (Huang, et al. 2015) is used to validate the triggered volume and to show the application of the tool. Limitations of the presented method are mentioned and ameliorations of the current model are proposed.

2 METHOD

The numerical simulation connects three successive 2D FEM models (see Figure 1), which allow to model the different phases of a mud flow:

1. Determination of the triggered volume by determining the failure mechanism in a numerical soil model of the slope in ZSOIL (ZSOIL 1985-2020)

2. Propagation of the triggered volume and impact on a building in TwoPhaseCode (Preisig and Zimmermann 2010)
3. Application of the impact force on a detailed non-linear structural model in ZSOIL
4. Quantification of the vulnerability based on an impact force-displacement curve

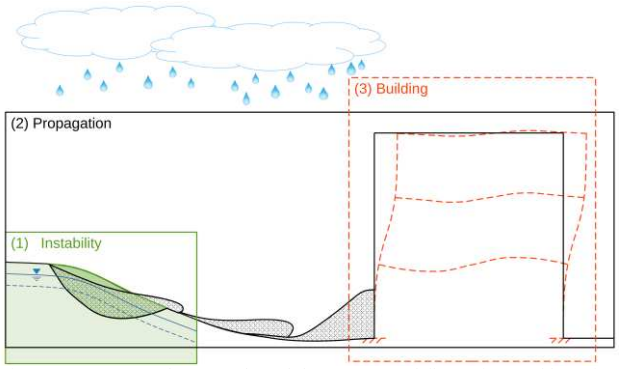

Figure 1. Process scheme and model scopes. Mud flow triggered by raise of groundwater level and impact on building. Model scopes: 1) instability triggered by raise of groundwater level, 2) propagation of the mud flow and 3) impact of the mud flow on a building

2.1 *First Model: Slope Instability*

A 2D plane strain model of the slope is introduced (ZSOIL 1985-2020). The model provided by the user includes the topology, stratigraphy (a constitutive model and soil parameters for each layer), a mesh and boundary conditions. The tool then adds a groundwater level at a chosen depth below surface. To consider preliminary information about the position slope failure, not all the slope between the failing region and the building has to be included in the scope of this model.

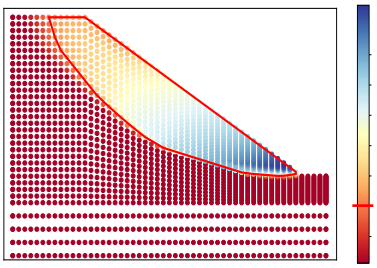

Figure 2. First model and results. Colormap: magnitude of relative displacement between last converged and first diverged step. Red line: failure mechanism determining triggered volume

A series of steady state flow analyses, each followed by a deformation analysis, are conducted while increasing the water level at each step. When a slope instability occurs, the displacements get very big and the deformation analysis fails to find a convergent solution. The results of the last iteration step are hence returned as divergent solution. A convex hull is drawn around the nodes, whose magnitude of the relative displacement between the last convergent solution and the divergent solution is bigger than a user chosen threshold (see Figure 2). The soil volume inside this hull is triggered as mud flow.

2.2 *Second Model: Propagation*

A second 2D FEM model simulating the propagation of the mud flow is introduced. The simulation software TwoPhaseCode (Preisig and Zimmermann 2010) conducts a 2D transient deformation analysis of a free surface flow. The flow is modelled as mixture of a solid phase s and a fluid phase f, both Newtonian fluids. Hence a linear relationship between the strain rate and the shear stress in each phase is assumed (see Figure 4).

The incompressible Navier-Stokes equations are solved for C_p, $\mathbf{v}_p$ and p on a triangular Lagrangian mesh, which adopts to the geometry in every time step, given ρ_p, $\mathbf{b}_p$, $\mathbf{g}_p$, $\mathbf{h}_p$, $\mathbf{v}_{p,0}$ and p_0, μ_p for index $p \in \{s, f\}$. The boundary value problem to be solved is given in Eqs. 1 - 8.

$$C_p\rho_p\frac{D\mathbf{v}_p}{Dt} = \nabla * \left(C_p\left(\sigma^d(\mathbf{v}_p) + p\mathbf{I}\right)\right) + C_p\rho_p\mathbf{b} \pm \mathbf{m}_{sf} \text{ on } \Omega \times]0,T[\quad (1)$$

$$0 = \nabla * (C_s\mathbf{v}_s) + \nabla * (C_f\mathbf{v}_f) \text{ on } \Omega \times]0,T[\quad (2)$$

$$\mathbf{m}_{sf} = K'_{drag}\left(\mathbf{v}_s - \mathbf{v}_f\right) \text{ on } \Omega \times]0,T[\quad (3)$$

$$\mathbf{v}_p = \mathbf{g}_p \text{ on } \partial\Omega_{g_p} \times]0,T[\quad (4)$$

$$\sigma_p * \mathbf{n} = \mathbf{h}_p \text{ on } \partial\Omega_{h_p} \times]0,T[\quad (5)$$

$$\mathbf{v}_p\,(t=0) = \boldsymbol{v}_{p,0} \text{ on } \Omega \quad (6)$$

$$\langle\sigma_p\rangle = C_p(\tau(\mathbf{v}_p) + p\mathbf{I}) \quad (7)$$

$$\tau(\mathbf{v}_p) = 2\mu_{N,p}\left(\dot{\varepsilon}(\mathbf{v}_p) - \frac{1}{3}(\nabla * \mathbf{v}_p)\mathbf{I}\right) \quad (8)$$

C_p is the volume fraction, $\mathbf{v}_p$ the velocity, ρ_p the density, $\tau(\mathbf{v}_p)$ the shear stress, p the pression, $\mathbf{b}_p$ the body force, $\mathbf{g}_p$ imposed displacements, $\mathbf{n}$ a normal vector, $\mathbf{h}_p$ surface tractions, σ_p the stress tensor, $\dot{\varepsilon}_p$ the shear strain rate and $\mu_{N,p}$ the dynamic viscosity of the fluid of each phase $p \in \{s, f\}$ and K'_{drag} a parameter taking into account the drag force $\mathbf{m}_{sf}$ between the phases.

De facto in TwoPhaseCode, the Dirichlet boundary conditions (see Eq. 4) are $v = 0$ conditions imposed on the nodes located on predefined linear line segments, hereafter referred to as boundary lines. These lines can be considered as rigid boundaries, as their position is constant in time and is independent of reactional forces. Boundary lines parallel to the axes can be either block transversal displacements ($v = 0$ parallel to the line) or allow them. So, these surfaces are either modelled as highly frictional ($v = 0$) or frictionless. As the boundary condition can exclusively be applied in axial direction, boundary lines skew to the axes can only be modelled as highly frictional. Concerning Neumann boundary conditions (see Eq. 5), the possibility to account for surface tension is implemented. Other surface tractions are not considered.

TwoPhaseCode returns the position, velocity, displacement, pressure and acceleration of each node in each time step.

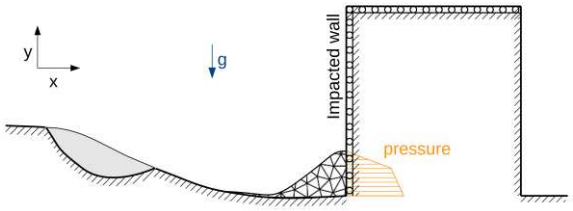

Figure 3. Second model. Black: boundary lines, possible boundary conditions: frictionless / full friction. Grey: initial step. At time t: Triangulated: position of material. Orange: pressure distribution on impacted wall.

Figure 3 shows a possible setup for the second model generated by the presented tool. The boundary lines are composed of the surface given in the first model, the bottom of the failure mechanism found in the same model and the hull around the building given in the third model. The part of the profile included in the scope of neither the first nor the third

model is included based on user input. At the building's downhill-side a runout plane is added. The wall facing uphill is defined as impacted wall.

By default, all boundaries are considered to be highly frictional. Boundaries parallel to the axes can be set to be frictionless manually.

In order to calculate the total impact force on the building, the pressures are integrated along the impacted wall. When the maximum force occurs, the pressure distribution along this wall is determined (see Figure 10).

In case the material's shear resistance is to be considered, as proposed by (Moriguchi, et al. 2009), the dynamic viscosity $\mu_{N,p}$ (see Eq. 8) can be calibrated on the problem, assuming the material to behave as a Bingham fluid. In this case a design point $(\dot{\gamma}^*,\ \tau^*)$ is chosen to minimize the error over the domain and the time between the Bingham and the Newtonian fluid (see Figure 4). Each Newtonian dynamic viscosity $\mu_{N,p}$ is then composed of a material component μ_B and a problem specific component $\tau_c/\dot{\gamma}^*$.

$$\mu_{N,\ p} = \frac{\tau_c}{\dot{\gamma}^*} + \mu_B \tag{9}$$

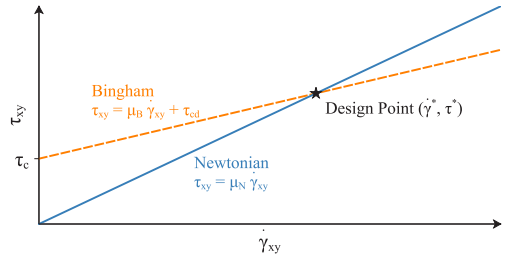

Figure 4. Constitutive relation of Newtonian fluid vs. Bingham fluid

2.3 *Third Model: Impact on building*

In ZSoil, the pressure distribution resulting from the second model is then applied on a 2D nonlinear structural model of the building provided by the user. This model includes material choice, a mesh, boundary conditions as well as any live or dead load acting on the building simultaneously to the mud flow. The pressure is then augmented up to the maximum total force determined in the previous step (see Figure 11). The model returns beside others, the displacements, forces and moments in the beams, plastic zones, etc.

2.4 *Quantification of Vulnerability*

An impact force - roof displacement diagram is then created (see Figure 13). The deformation is used to classify the vulnerability as follows:

- Elastic deformation: no or little damage on structural elements
- Plastic deformations: medium damage
- Collapse: considerable damage

3 VERIFICATION OF PROPAGATION MODE

(Moriguchi, et al. 2009) conducted a set of small-scale experiments on dry fine sand. The sand, released from a rectangular box, propagated down an inclined rectangular flume. The impact force time history on a rigid obstacle placed at the end of the channel (see Figure 5) was measured. Additionally, the propagation was filmed through the side of the channel. The experiment was conducted on channel inclinations from 45°- 65°.

The same group calibrated a SPH-model on the experimental results, modelling the sand as Bingham fluid. The material properties are shown in Table 1. They showed, that the mentioned model can predict the time history of the impact force, from the peak value up to the quasi-static residual force.

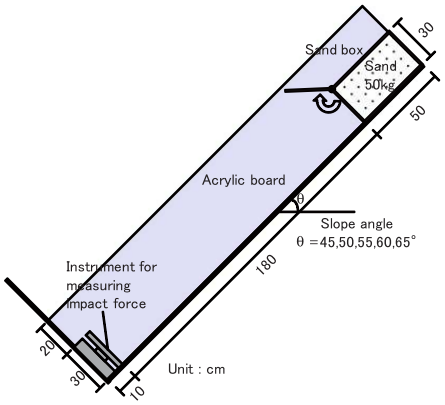

Figure 5. Schematic illustration of the experimental setup (Moriguchi, et al. 2009)

We set up a propagation model (see section 2.2) of the experiment according to fig. 6, modelling the sand as single-phase fluid by assuming the same material properties in both phases. The boundary line representing the back of the wall was assumed to be frictionless, all other boundary lines were modelled as highly frictional.

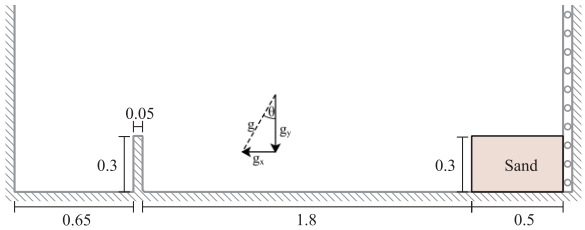

Figure 6. Scheme of the model for the transient deformation analysis (see section 2.2)

Table 1. Material properties of dry sand, assuming a Bingham fluid

Viscosity	η_B $[Pa \cdot s]$	1.0
Friction angle	φ [°]	41.0
Cohesion	c $[kPa]$	0
Density	ρ $[kg/m^3]$	1379

We calibrated our propagation model on the experimental results. In a first step, the equivalent Newtonian viscosity was estimated on the expected impact time as shown in Eqs. 10 and 11, applying a Mohr-Coulomb failure criterion.

$$\dot{\gamma}^* = \frac{1.80m}{0.3m * t_{arrival}} \tag{10}$$

$$\mu_N = \frac{p*\tan(\varphi) + c}{\dot{\gamma}^*} + \mu_B \tag{11}$$

The Newtonian viscosity μ_N was chosen to satisfy Eq. 10, with p being the mean pressure in a chosen representative time step. In a second step, a fine calibration of the μ_N on the maximum impact force was conducted.

After its release the material propagates down the flume. The arrival of the front at the obstacle results in an abrupt halt of most of the material, resulting in a fast increase in impact force. The maximum impact force is reached shortly after the initial impact. It increases with an increasing slope angle θ, (see Figure 8). With an increasing inclination angle θ, the increase of impact force gets faster and the delay of the maximum impact gets shorter. After the maximum impact, the impact force decreases slower than the increase rate before stagnating at a value close to the hydrostatic force. This force does not depend on the flume

inclination.

The simulated force time histories follow the same pattern, with the following differences to the experimental results. The impact occurs later in the numerical simulation. On the other hand, the impact force increases at a much higher rate in the numerical simulation. There is no visible pattern in the delay of the maximum impact with respect to the experimental results. Notably, the residual force of the simulation is lower than the measured one, especially for high inclination angles. For shear velocities lower than the design velocity $\dot{\gamma}^*$ the viscosity of the Newtonian fluid is lower with respect to other models. Stopping mechanisms of the fluid are therefore underestimated, which leads to more spilled over material, because the material does not stop before. This corresponds to a larger amount of material spilled over the obstacle.

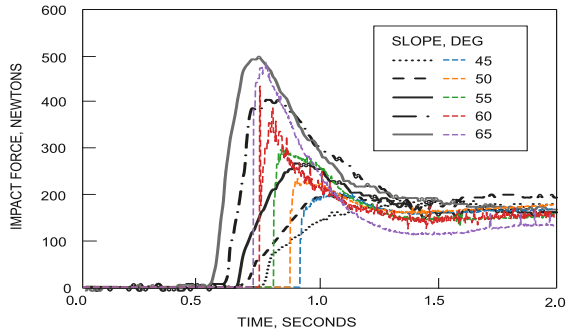

Figure 7. Time history of the impact force. Grey scales: experimental results (Moriguchi, et al. 2009). Colours: our numerical results

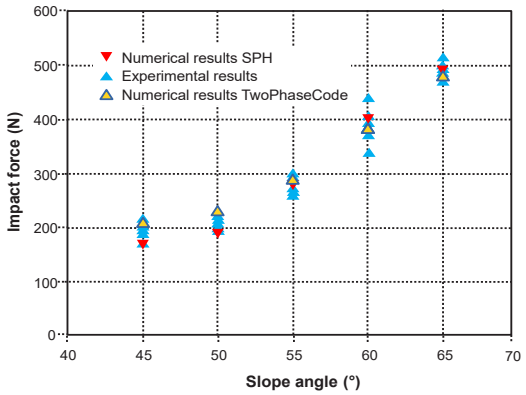

Figure 8. Max. impact force measured and predicted by (Dai, et al. 2017). TwoPhaseCode: our propagation model

The peak value as well as the post-peak behaviour, including the quasi-static residual force were captured sufficiently accurate, when calibrated accordingly.

4 CASE STUDY: WENJIA GULLY

The 2008 Wenchuan earthquake triggered a landslide in Wenjia Gully (Sichuan Province, China) and left approximately $30 * 10^6\ m^3$ of loose material. On August 2010 this deposit began to move due to a heavy rainfall. Propagating downhill, it hit several check-dams in the gully. (Dai, et al. 2017)

(Huang, et al. 2015) found a profile of the triggered volume by comparing the ground surface before and after the event (see Figure 9). They also calibrated a SPH-model of the event (see Table 2), assuming a Bingham constitutive law.

Table 2. Material properties proposed by (Dai, et al. 2017).

Viscosity	$\eta_B\ [Pa \cdot s]$	136.0
Friction angle	$\varphi\ [°]$	34.0
Cohesion	$c\ [kPa]$	0.8
Density	$\varrho\ [kg/m^3\ ]$	2100

In this paper, we validate the triggered volume. This volume is then propagated down the slope. The impact force on the first check dam is evaluated and is imposed on three fictive buildings replacing the check dam.

The proposed initial surface geometry was simplified. A slope model (see section 2.1) was created, assuming a Mohr-Coulomb failure criterium for the deposed material.

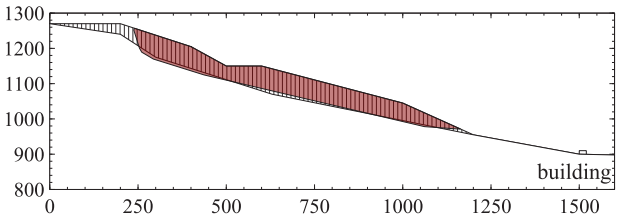

Figure 9. Found mechanism of rupture: our prototype (red), mechanism proposed by (Huang, et al. 2015) by a comparison of the initial surface to the surface after the event (hatched)

As shown in Figure 9, the proposed mechanism of rupture can be reproduced with our instability model, with a relative volume error of about 9%. The activation of the top part, which was not covered by the failure mechanism can be explained by a local weakness, which was not considered.

The found volume is propagated down the slope using a propagation model, considering all boundary lines as highly frictional, except for the top of the building, which is modelled as frictionless.

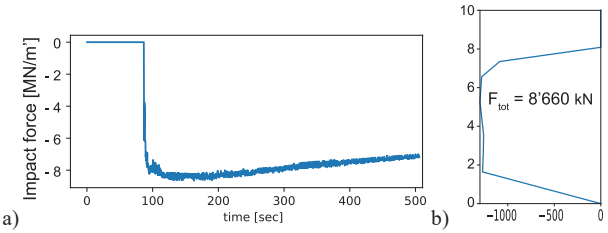

Figure 10. a) Evolution of the impact force on the building, b) pressure distribution on the impacted wall at the maximum impact [kN/m^2].

A single dynamic viscosity μ_N is assumed for both phases. It is calibrated in a trial and error process on the expected arrival time of $t_{arrival} = 100\ sec$. In a backward analysis, it could be shown, that the difference between the viscosity derived by Eq. 11 ($\mu_N \approx 5.1 - 5.9 \cdot 10^6 Pa \cdot s$) and the chosen viscosity ($\mu_N = 1.0 \cdot 10^6 Pa \cdot s$) is less than an order of magnitude.

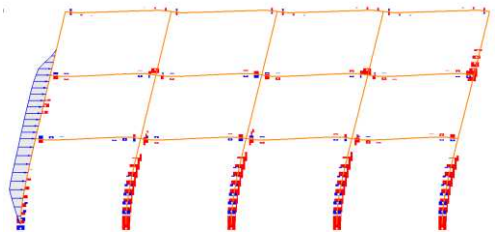

Figure 11. Structural model of the fictive building with medium damages. Impact pressure, deformation and plastic zones.

Figure 10a) shows the evolution of the impact force and Figure 10b) the maximum impact pressure. This pressure distribution is applied on three fictive buildings, each with the same geometry (see Figure 11) and boundary conditions. Depending on the constitutive models and material properties, the buildings show different behaviours under the load. For simplicity, only the material's constitutive laws are altered from elastic-perfectly plastic to elastic between the models.

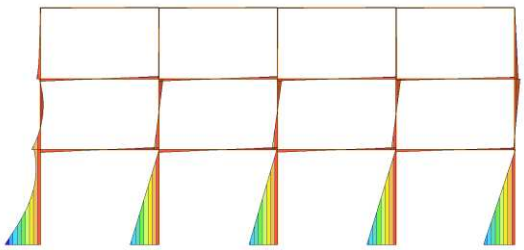

Figure 12. Moment diagram of impact force imposed on a building with medium damages.

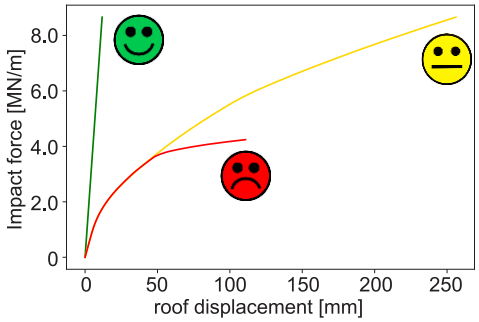

Figure 13. impact force - roof displacement diagram of a building with little or no (green), medium (yellow) and considerable (red) structural damage

Figures 11 and 12 show possible results of the deformation analysis of a building with medium damages, when impacted by the maximum impact force. Figure 13 shows the impact force – roof displacement curves of the three fictive buildings mentioned above. The presented results provide a basis for the vulnerability of the given building and the design of protection measures.

5 LIMITATIONS

With long slopes and a shallow ground water level, numerical errors are likely to occur during the flow step of the first model. Choosing an appropriate scope for the first model can help to avoid them, but also the plausibility of the resulting groundwater level has to be examined carefully.

To calculate the impact force with an acceptable accuracy with the current algorithm, the mesh size of the fluid in the propagation model has to be sufficiently small (maximum side length < 0.2*wall's height). As this parameter influences the mesh density of all the fluid, it has a non-neglectable influence on the computational effort of this calculation step. To avoid slip through errors (see section 5.1), acute angles are avoided by cutting them with additional boundary lines. Alternatively, the length of the time steps can be adjusted.

Whether the simplification of the fluid as Newtonian fluid is appropriate depends on the problem's homogeneity and constancy. The bigger the differences in terms of shear velocity and material parameters over time and over space are, the bigger the error by assuming a single viscosity gets.

The presented models are in 2D. For buildings relatively slender in comparison to the width of the mud flow or with an impacted wall facing skew to the mud flow, important effects are neglected. Also, the influence of a curved flow path cannot be captured.

5.1 *Numerical Errors of the second model*

In the propagation model, there are some unresolved numerical issues around the boundaries. They are mostly caused by the method used to determine the boundary (Preisig and Zimmermann 2010). In each timestep:

1. The nodes move
2. Project the nodes close to a boundary line onto it, if they are situated on its negative side
3. Determine an α-shape (Da 2020) around the nodes. This is the boundary consisting of boundary-nodes and boundary-segments
4. Re-mesh and re-triangulate the area inside the boundary

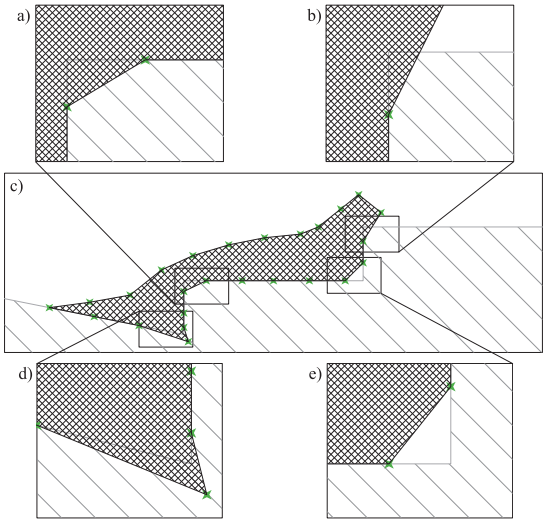

Figure 14. Numerical errors. a, b) Cutting of the outer edge, d) slipping through the edge and e) cutting of the inner edge

The following errors can occur, following this method:

The cutting of the outer edge shown in Figure 14a) and b) can occur, because the α-shape algorithm does not account for the boundary lines being intersected. This can lead to various problems, from not capturing the pressure on the upper edge of the building, to not measuring any force on the building at all, to even loosing fluid volume through the building floor.

The cutting of the inner edge shown in Figure 14e) occurs, when a boundary segment connects two boundary lines, which impose zero velocity in both directions. Having no reason to add a node on this segment, this hole persists in time.

The slipping through error (see Figure 14d), Figure 15) appears, when a node moves to a position, wherefrom it cannot be projected on a boundary line.

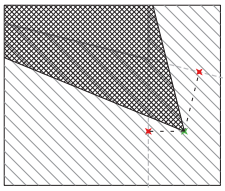

Figure 15. Timestep after slipping through edge error. The boundary node cannot be projected on any of the boundary Lines.

The following procedure is proposed to avoid these errors:

1. The nodes move
2. Project the nodes close to a boundary line onto it, if they are situated on its negative side
3. Determine an α-shape around the nodes. This is the boundary consisting of boundary-nodes and boundary-segments

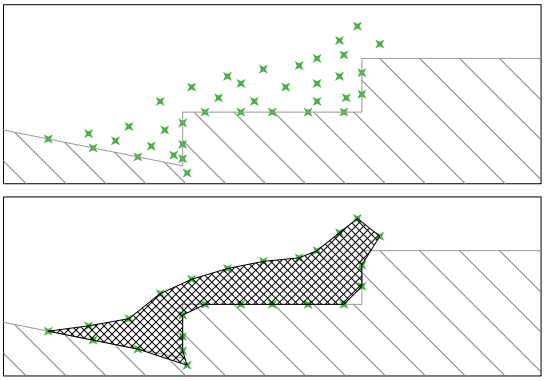

4. Simplify the boundary, by merging inline segments

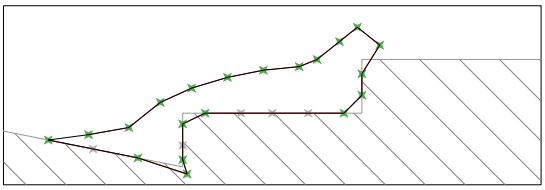

5. Add the intersection points of boundary lines and boundary segments

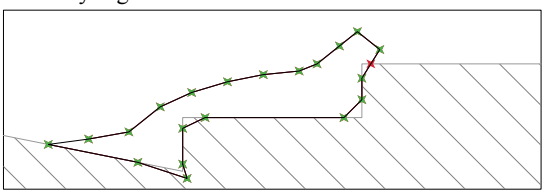

6. Add the centre of boundary segments connecting two boundary lines

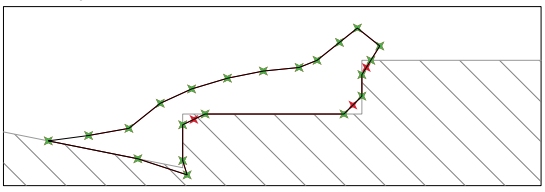

7. If neighbours of a boundary node are situated on two different boundary lines and it is situated on the negative side of the boundary lines, move the node to the intersection of these lines

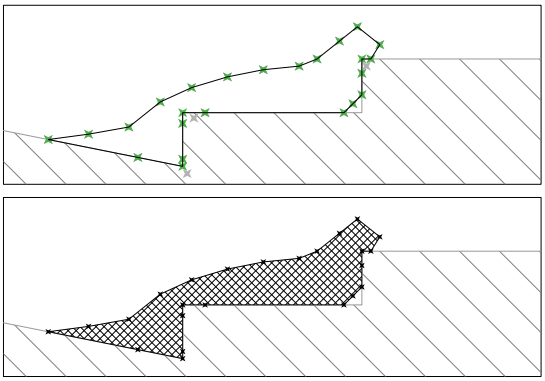

8. Re-mesh and re-triangulate the area inside the boundary

6 CONCLUSIONS AND OUTLOOK

The results of a small-scale experiment were used to show, that the presented model is able to predict the evolution of the impact force on a rigid obstacle of granular material. A calibration method for the dynamic viscosity was introduced, depending on the problem's geometry and material properties.

The real-life example of the 2010 event in Wenjia Gully, China was modelled. The activated material could be reproduced numerically. The force on a fictive building, placed in the gully was simulated and then applied on three structural models of the building. Based on the numerical results, the building's vulnerability can be estimated.

The prototype tool can be used to predict the vulnerability due to a mud flow, given a good calibration. Nevertheless, certain material effects, such as the interdependency between viscosity and shear velocity cannot be captured by the presented model.

Exploring further constitutive models and the corresponding calibration can improve not only the model with respect to mud flows, but can allow the tool to model debris flows in the same vein. Other possible changes on the 2D model concentrate on the second model. The presented algorithm (see section 5.1) can be implemented to reduce the occurrence of numerical errors. Further the definition of boundary lines could be altered in order for them to allow a frictional behaviour. An expansion of the model in three dimensions would include major changes in the second model as well as in the interface between the models and the tool.

7 ACKNOWLEDGEMENTS

This project was supported by the research program "Nature et Ville". We thank M. Preisig for the help regarding the application of the second FEM model.

8 REFERENCES

Blahut, J., Glade, T., and Sterlacchini, S. 2014. Debris flows risk analysis and direct loss estimation: the case study of Valtellina di Tirano, Italy. *Journal of Mountain Science* (Springer) 11(2), 288-307.

Cardinali, M., et al. 2002. A geomorphological approach to the estimation of landslide hazards and risks in Umbria, Central Italy.

Ciurean, R. L., et al. 2017. Multi-scale debris flow vulnerability assessment and direct loss estimation of buildings in the Eastern Italian Alps. *Natural hazards* (Springer) 85(2), 929-957.

Da, T. K. F. 2020. 2D Alpha Shapes. *CGAL User and Reference Manual.* 5.1.1 edition. CGAL Editorial Board.

Dai, Z., Huang, Y., Cheng, H., and Xu, Q. 2016. SPH model for fluid–structure interaction and its application to debris flow impact estimation. *Landslides* (Springer) 14(3), 917-928.

Fuchs, S., Heiss, K., and Hübl, J. 2007. Towards an empirical vulnerability function for use in debris flow risk assessment. *Nat. Hazards Earth Syst. Sci.*, 7, 495–506.

Huang, Y., et al. 2015. SPH-based numerical simulation of catastrophic debris flows after the 2008 Wenchuan earthquake. *Bulletin of Engineering Geology and the Environment* (Springer) 74(4), 1137-1151.

Mavrouli, O., et al. 2014. Vulnerability assessment for reinforced concrete buildings exposed to landslides. *Bulletin of engineering geology and the environment* (Springer) 73(2), 265-289.

Moriguchi, S., Borja, R. I., Yashima, A., and Sawada, K. 2009. Estimating the impact force generated by granular flow on a rigid obstruction. *Acta Geotech*. 4, 57-71. Berlin Heidelberg: Springer-Verlag.

Preisig, M., and Zimmermann, T. 2010. Two-phase free-surface fluid dynamics on moving domains. *Journal of Computational Physics* (Elsevier) 229(7), 2740-2758.

ZSOIL. User manual ZSoil®.PC v2020. Soil, Rock and Structural Mechanics in dry or partially saturated media. ZACE Services Ltd, Lausanne, Switzerland, Switzerland, 1985-2020.